J Mater Sci (2020) 55:15867–15881

Electronic materials

Effect of carboxymethyl cellulose on the flow behavior of lithium-ion battery anode slurries and the electrical as well as mechanical properties of corresponding dry layers

Ronald Gordon[1,*], Raquel Orias[1], and Norbert Willenbacher[1]

[1] *Institute of Mechanical Process Engineering and Mechanics – Applied Mechanics Group, Karlsruhe Institute of Technology (KIT), Gotthard-Franz-Str. 3, 76131 Karlsruhe, Germany*

Received: 11 May 2020
Accepted: 17 August 2020
Published online: 27 August 2020

ABSTRACT

We present a holistic view on the role of polymeric binders in waterborne LiB anodes, including preparation and processing of wet slurries as well as microstructure, electrical conductivity and mechanical integrity of dry electrode layers. We focus on carboxymethyl cellulose (CMC), with respect to technical application the influence of soft, nano-particulate styrene–butadiene rubber (SBR) as secondary binder is also addressed. We discuss the influence of CMC concentration, molecular weight (M_w) and degree of substitution (DS) on flow behavior of anode slurries. Rheological data are not only relevant for processing, here we use them to characterize the adsorption of CMC on active material particles and dispersion of these particles in the slurry at technically relevant concentrations. The fraction of CMC adsorbed onto graphite particles increases with increasing M_w and decreasing DS. Electrical conductivity increases with M_w, i.e. with decreasing free polymer deteriorating conductive carbon black pathways. CMC does not contribute to the adhesion of electrode layers, irrespective of M_w or DS, technically feasible adhesion is inferred by SBR. Cohesive strength of anode layers, determined here for the first time under well-defined mechanical load, increases with increasing M_w and decreasing DS, i.e. with increasing fraction of adsorbed CMC and corresponding improved particle dispersion. Strong cohesion and high electrical conductivity are correlated to an alignment of graphite particles as revealed by electron microscopy, presumably enabled by higher particle mobility in well-dispersed slurries. Accordingly, targeted choice of CMC is a valuable means to control processing, electrical conductivity and mechanical strength of LiB electrodes.

Handling Editor: David Cann.

Address correspondence to E-mail: ronald.gordon@kit.edu

https://doi.org/10.1007/s10853-020-05122-3

Introduction

Lithium-ion batteries (LiB) play an important role as electrochemical energy storage systems. They combine high energy and power density, making them suitable for portable electronics, hybrid/full electric vehicles and grid applications [1–5]. So far, research mainly focused on the development of new electrochemically active materials to achieve high cell performance [6–10]. In contrast, little attention has been paid to the role of binders not only for processing but also for the performance of LiB. As electrochemically inactive material, poly (vinylidene fluoride) is one of the most widely used polymeric binders for LiB electrodes. Conventionally, these binders are dissolved in organic solvents, such as *N*-methyl-2-pyrrolidone (NMP) [11, 12]. Since organic solvents are typically environmentally unfriendly and flammable, safety concerns and high cost are associated to their use in LiB production, particularly for the upcoming high-volume mass production of electric vehicles. Therefore, water-based electrodes have been developed as promising environmentally benign alternative [13, 14].

Carboxymethyl cellulose (CMC) and styrene butadiene rubber (SBR) are often combined as additives for aqueous anode slurries to achieve high stability and processability as well as superior electrochemical cell performance [15–20]. The present investigation focuses on CMC as binder. Additionally, nano-scale SBR particles are added during slurry preparation since this soft, rubber-like polymer is necessary to provide a technically feasible adhesion to the current collector. CMC is a linear, long-chain, water-soluble, anionic polysaccharide, consisting of two anhydroglucose units (β-linked glucopyranose residues) with three hydroxyl groups each. The hydrogen in the hydroxyl groups can be substituted by a carboxymethyl group ($-OCH_2COO^-$). The average number of substituted hydroxyl groups per anhydroglucose unit is defined as the degree of substitution (DS) and hence has a maximum of 3. Rheological properties of CMC solutions strongly depend on concentration, molecular weight (M_w), DS and pH [21–26]. This also shows up in the flow behavior of battery electrode slurries. Beyond that, however, the interaction with other components in these slurries has to be considered. Lee et al. investigated the effect of CMC DS on the dispersion of graphite particles and the resulting electrochemical performance of corresponding anodes [16]. CMC with lower DS adsorbed preferentially on graphite, dispersing the particles and stabilizing the slurry against sedimentation through repulsive electrosteric interparticle forces. As a result, longer cycle life and improved electrochemical cell performance was achieved using low substituted CMC. Other studies have shown the effect of polymeric binders on particle dispersion, unveiling their influence on the electrical conductivity of electrode layers [27–29]. Proper binder to particle ratios and dispersion properties of the binder lead to the formation of a conducting network, enhancing the electron transport kinetics and yielding higher energy, power and life time performance.

Battery lifetime strongly depends on the mechanical integrity of the dry electrode. During lithium intercalation, the electrode must withstand mechanical stresses due to expansion and shrinkage of the electrochemically active material [30–32]. The volume fluctuations can induce a local delamination of the electrode layer from the current collector and cracking within the layer. Hence, considerable research work dealt with the determination of adhesive strength between electrode layer and substrate [17, 33–46]. However, the cohesive strength in the electrode layer has not received much attention yet. The scratch test has been used to characterize the mechanical strength or scratch resistance of electrodes [33, 47, 48]. Since in this test the electrode layer experiences tangential and normal forces, the measured load comprises information about the adhesive as well as the cohesive strength of the electrode. Chen et al. combined micro-scratch and digital image correlation techniques to decouple particle/particle cohesion from electrode-layer/current-collector adhesion and defined the coefficient of friction as a measure of cohesive strength [49]. Nevertheless, it remains elusive whether such local force measurements are representative for the cohesive strength of the electrode layer. Finally, indentation and tensile tests have been carried out to determine the mechanical properties of electrode layers [37, 50–52]. These studies provided some understanding about how wet processing of the slurry affects porosity and mechanical properties of the dry layer. Still, the true contribution of the binder to the cohesive strength of electrode layers is not yet fully resolved.

In this study we present a holistic view on the role of polymeric binders for LiB anodes, including

preparation and processing of wet slurries as well as the microstructure, electrical conductivity and mechanical integrity of dry electrode layers. We first investigate the influence of CMC concentration, molecular weight and degree of substitution on flow behavior of aqueous anode slurries. Rheological data are not only relevant to judge processing behavior, here we use them to characterize the degree of adsorption of CMC on active material particles and the degree of dispersion of these particles in the slurry at technically relevant concentrations. The slurries are then cast on to glass plates and copper foils and dried to determine the electrical conductivity and the adhesive strength of the electrode layer, respectively. Furthermore, first cohesive strength data for thick anode layers comprising graphite, carbon black and CMC are presented. The adsorption behavior of CMC on the particle surface is discussed and correlated to the obtained results. Finally, we present data characterizing the cohesive strength of anode layers under well-defined mechanical load conditions for the first time and correlate these data to the electrode microstructure and its change with varying type and concentration of CMC, emphasizing its relevance for the mechanical integrity of the electrode layer beyond the mere presence of the polymeric binder. With respect to the typical composition of commercial LiB electrodes, the influence of two different SBR-binders on the mechanical, structural and electrical properties mentioned above is also discussed.

Experimental

Materials

Commercially available flake-like, synthetic graphite particles (SLP50, Imerys Graphite & Carbon, Switzerland) with a volume-based average diameter $x_{50,3}$ = 23 µm, a specific surface area of 5.7 $m^2\ g^{-1}$ and density of 2.25 g cm^{-3} are used as active material for the preparation of aqueous anode slurries. Carbon black (CB, C-Nergy Super C65, Imerys Graphite & Carbon, Switzerland) with a primary particle size $x_{50,3}$ = 32 nm, a specific surface area of 64.1 $m^2\ g^{-1}$ and density of 1.8 g cm^{-3} was added as a conductivity agent. CB particles tend to agglomerate in the slurry reaching an average agglomerate size of 5 µm. Four types of sodium carboxymethyl cellulose (CMC, Sigma Aldrich, Germany) with average molecular weight (M_w) of 250 kDa and 700 kDa were used in this investigation. The latter had a degree of substitution (DS) of 0.9, whereas three different DS of 0.7, 0.9 and 1.2 were investigated for CMC with M_w = 250 kDa. Additionally, CMC with M_w = 400 kDa and DS = 0.9 was purchased from Dow Wolff Cellulosics GmbH. Commercially available styrene butadiene rubber (SBR, TRD2001, JSR Micro NV., Belgium) as well as a modified version (TRD105A) were used as secondary binder. These polymers are supplied as aqueous dispersions of nanoparticles (particle volume fraction 48 vol% and 41 vol% for TRD2001 and TRD105A, respectively). According to manufacturer, TRD2001 exhibits a particle size of 170 nm and a glass transition temperature of − 2 °C, whereas TRD105A has a particle size of 95 nm and a glass transition temperature of − 5 °C. Small amplitude oscillatory shear experiments at fixed frequency and deformation covering a wide temperature range on dry SBR films did not show a cross-over of the storage (G') and loss (G'') moduli at high temperatures, indicating high molecular weight of the polymers or even chemical cross-linking (see supporting information). Gravimetric measurements using toluene as solvent yielded a degree of cross-linking of 89.9% ± 0.5% and 81.5% ± 0.4% for TRD2001 and TRD105A, respectively.

Sample preparation

Anode slurries with a constant solid volume fraction ϕ_p = 20 vol% and a constant graphite to CB volume ratio of 46.5 were studied. The CMC concentration was varied in a range ϕ_{CMC} = 2.5–4.0 vol% for different molecular weight and degree of substitution. Here, ϕ_{CMC} refers to the amount of polymer in the dry electrode layer. First, CMC was dissolved in distilled water and homogenized with a 55 mm propeller mixer at 1200 rpm for 30 min. Carbon black, followed by graphite particles, were dispersed in the aqueous CMC solution using a 50 mm dissolver disk at 1600 rpm for 5 min each. Only part of the total amount of water needed for the slurry was initially used to prepare the CMC solution in order to ensure particle deagglomeration and ideal slurry homogeneity. After addition of the solid particles, the remaining amount of water was added stepwise in four intervals of 5 min each until reaching the desired solids content [53]. For anode slurries including SBR,

the secondary polymer was added after dispersion of the solid particles and finally the desired solids content was adjusted by adding the appropriate amount of water. Slurries including both polymer binders were studied at fixed CMC concentration ϕ_{CMC} = 2.5 vol% and constant M_w = 700 kDa and DS = 0.9 but varying SBR concentration in a range ϕ_{SBR} = 1.0–5.0 vol%.

Slurries were coated on glass plates and 10 µm thick copper foil (SE-Cu, Schlenk Metallfolien GmbH & Co. KG, Germany) for electrical conductivity and adhesive strength measurements, respectively. Therefore, a doctor blade (ZUA 2000, Zehntner GmbH, Switzerland) with a coating width of 60 mm and a coating gap of 300 µm was applied. Subsequently, the wet film was dried at 60 °C for 30 min. Additionally, thick electrode layers were prepared for the determination of the cohesive strength in the dry electrode layer. Slurries were poured into a 26 × 49 × 11 mm^3 ($W \times L \times H$) silicone mold and dried at 60 °C for 24 h, during the first 3 h of drying an aluminum foil covered one third of the area to suppress the Marangoni effect. The dry layers were then cut and grinded into smaller samples with defined shape. First, the samples were brought into shape using sandpaper with rough texture and then smoothed applying fine sandpaper. Different sample shapes were used to determine the cohesive strength of the electrode layer depending on the applied load type as summarized in Table 1.

Sample characterization

Rheological measurements

The flow behavior of the anode slurries was characterized applying rotational steady shear measurements. A stress controlled rheometer (Physica, MCR 501, Anton Paar GmbH, Germany) was used to determine the viscosity η in the shear stress range 0.1 Pa < τ < 1000 Pa. All measurements were performed with a 5 min waiting period before starting the measurement to ensure structure recovery using a 25 mm diameter plate-plate geometry and 1 mm gap width at 20 °C.

Table 1 Sample geometry for cohesion testing

Load type	Sample width (mm)	Sample length (mm)
Compression	5	5
Flexural	20	45
Tensile*	5	24
Torsion	9	35

All samples had a height of 1.5 mm

*Dog bone test samples: width at the middle of the sample, length between device clamps

Electrical conductivity tests

The four-point resistivity test was conducted on a self-manufactured set-up equipped with four measuring probes (S4D5G, Uwe Electronic GmbH, Germany). Measurements were carried out at five different positions of the 60 mm × 120 mm anode layer applying five different currents and recording the corresponding voltage. An average value of the electrical conductivity was calculated for a probe spacing of 30 mm according to Smits [54].

Mechanical properties

The adhesive strength of the electrode layer to the copper foil was characterized using a 90°-peel-test based on the standard DIN 28510-1. A universal testing machine (Texture Analyzer TA.XT plus, Stable Micro Systems, UK) was used to peel off the copper foil. Specimen with a width of 25 mm and a length of 60 mm were fixed to the measuring plate with double-sided adhesive tape (Universal, Tesa SE, Germany). A 500 g plate was set on top of the electrode layer as a pre-compression step to ensure homogeneous contact between adhesive tape and electrode layer. All measurements were performed at a constant peel velocity of 5 mm s^{-1} using a 5 kg load cell force sensor (max. force: 5 kg, force sensitivity: 0.1 g). The measured tensile force was normalized to the line width. This line load was used as a measure for adhesive strength.

The cohesive strength of the electrode layer was determined employing standard test methods for the characterization of mechanical properties. Compressive $\sigma_{c,max}$ and flexural strength $\sigma_{b,max}$ (4-point bending) measurements were conducted using a universal testing machine (Texture Analyzer TA.XT plus, Stable Micro Systems, UK) based on the standard DIN 51104 and DIN 843-1, respectively. Additionally, tensile strength $\sigma_{t,max}$ tests were carried out using custom-made measuring fixtures and DIN ISO

EN 527-4 based sample geometries. Further, the torsional strength $\sigma_{tor,max}$ was obtained from dynamic mechanical analysis using a stress-controlled rheometer (Physica, MCR 301, Anton Paar GmbH, Germany) equipped with a 12 mm solid rectangular fixture (SRF 12). Therefore, oscillatory stress-sweep measurements were carried out at a constant frequency of 0.1 Hz until exceeding the destruction-free linear viscoelastic region, indicating the maximum torsional strength of the sample.

Microstructure

The porosity ε of the electrode layers was determined from the Archimedes density according to DIN EN 993-1 and DIN EN 993-18. Samples of dry electrodes were vacuum infused with epoxy resin, grinded with SiC paper and polished with a diamond suspension to investigate the microstructure of the electrode layers by means of scanning electron microscopy (SEM) using a LEO1530 microscope (Carl Zeiss AG, Germany).

Results and discussion

Rheological characterization

The viscosity η of anode slurries with and without CB as a function of the shear stress τ was compared to that of corresponding pure CMC solutions to characterize their flow behavior and the influence of solid particles on the rheological properties of the slurries. Figure 1 shows such flow curves for slurries including CMC with M_w = 700 kDa and DS = 0.9 at ϕ_{CMC} = 4 vol%. The CMC concentration refers to the amount of CMC in the dry electrode layer. The slurries show higher viscosity than the pure CMC solution. The relative viscosity $\eta_{rel} = \eta_{slurry}/\eta_{solution}$ for the slurry comprising graphite and CB is $\eta_{rel} \approx$ 2–3 throughout the investigated shear stress range as expected for well dispersed non-Brownian hard sphere suspensions with ϕ_p = 20 vol% [55]. For the slurry containing only graphite, the low shear viscosity is substantially higher ($\eta_{rel} \approx 10$), indicating incomplete dispersion of particles, i.e. agglomerates immobilizing part of the solvent still exist. At high shear stresses these agglomerates are broken up due to sufficient energy input and the viscosity of both slurries matches.

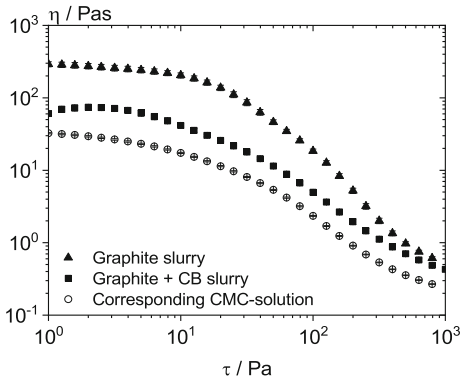

Figure 1 Viscosity as a function of shear stress for anode slurries with and without CB as well as the corresponding CMC solution. The particle loading of the slurries is ϕ_p = 20 vol%. The aqueous CMC solution includes 4 vol% CMC with M_w = 700 kDa and DS = 0.9.

The influence of DS and M_w of CMC on the low shear (τ = 1 Pa) and high shear (τ = 500 Pa) viscosity of anode slurries was investigated at different CMC concentrations. The low shear viscosity provides information about the particle dispersion in the slurry, whereas the high shear viscosity at constant ϕ_p reflects the amount of CMC dissolved in the fluid phase. The low shear viscosity as well as the high shear viscosity values of anode slurries slightly increase with increasing DS at constant M_w, suggesting that a lower DS results in slightly better particle dispersion and lower amount of free CMC in the fluid phase (see supporting information) as expected due to the higher degree of CMC adsorption on particle surfaces at low DS [16].

The low and high shear viscosity of slurries at different ϕ_{CMC} and constant DS = 0.9 is displayed as a function of M_w in Fig. 2a and b, respectively. Instead of a monotonic increase of viscosity with M_w according to a superior thickening efficiency of longer polymer chains we find, that both low and high shear viscosity increases with increasing M_w up to 400 kDa and then levels off for all investigated ϕ_{CMC} [56]. This result can be related to the adsorption behavior of CMC on graphite and CB particles. To gain better insight into the M_w dependence of CMC adsorption on the suspended particles, the relative viscosity at high shear stress (τ = 500 Pa) $\eta_{rel,\infty} = \eta_{\infty,suspension}/\eta_{\infty,solvent}$ was plotted against M_w as shown in Fig. 2c. The characterization of the CMC adsorption behavior using this rheological

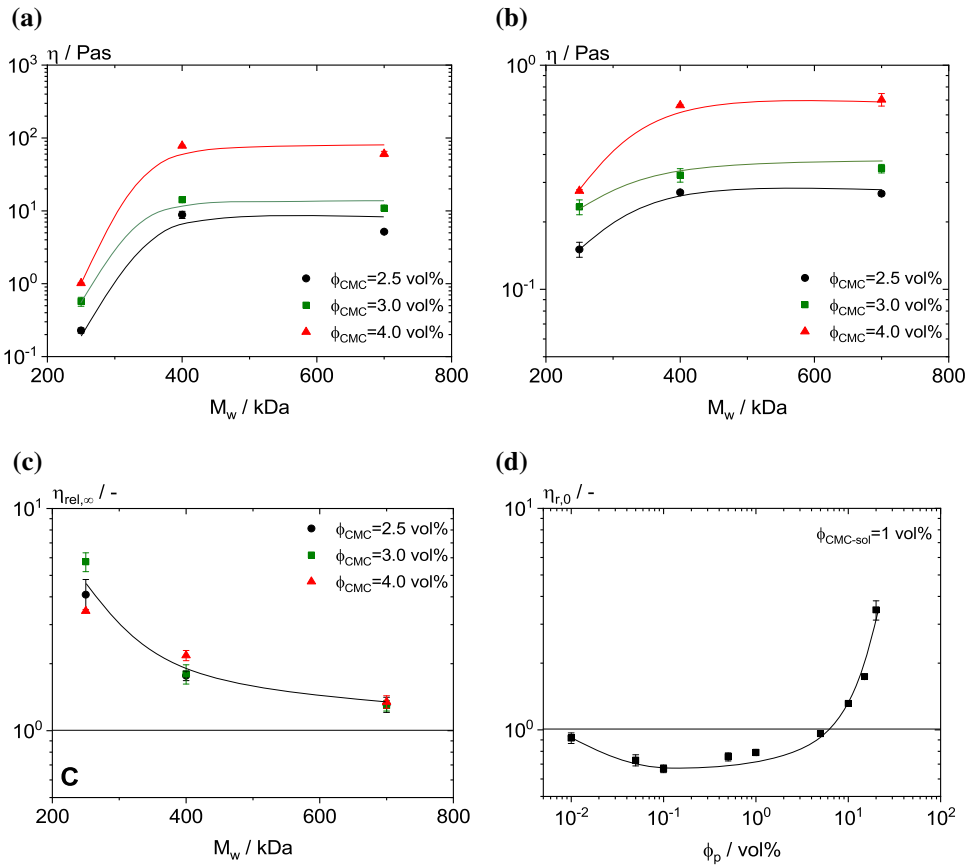

Figure 2 Viscosity of anode slurries at **a** low (τ = 1 Pa) and **b** high (τ = 500 Pa) shear stresses vs. molecular weight of added CMC (DS = 0.9). **c** shows the relative high shear viscosity $\eta_{rel,\infty}$ calculated from the data shown in (**b**) and the corresponding viscosity data for the respective CMC solutions. Slurries with different amount of CMC but at constant ϕ_p = 20 vol% were investigated. **d** Relative zero shear viscosity $\eta_{r,0}$ of graphite suspensions as function of particle loading ϕ_p. Graphite particles were suspended in an aqueous 1 vol% CMC solution with M_w = 700 kDa and DS = 0.9.

approach renders a significant advantage over common techniques like optical methods or adsorption isotherms, which require highly dilute systems. In contrast, rheological measurements enable the determination of CMC adsorption on the solid particles surface at technically relevant particle loadings. The relative high shear viscosity $\eta_{rel,\infty}$ monotonically decreases with increasing M_w, indicating a reduced fraction of free polymer in the solvent when using high M_w CMC. Consequently, the high shear viscosity of the slurry does not increase monotonically with M_w. Obviously, the effect of reduced free polymer in solution outweighs the slight increase in effective ϕ_p due to the CMC adsorption layer and the effect is independent of ϕ_{CMC} in the concentration range investigated here. It must be noted that the addition of SBR does not affect the flow behavior of the slurry. The contribution of the SBR nanoparticles to the overall particle volume fraction is negligible in relation to the active material content.

To shed more light on the adsorption behavior of CMC on graphite particles a series of graphite suspensions with ϕ_p ranging from 10^{-2} to 20 vol% was investigated with respect to their zero-shear viscosity $\eta_{0,suspension}$ normalized to the zero-shear viscosity $\eta_{0,solvent}$ of the used solvent, an aqueous 1 vol% CMC (M_w = 700 kDa, DS = 0.9) solution. The selected CMC concentration allows for a conclusive investigation of the adsorption behavior since higher concentrations result in a weaker change in relative viscosity, since a high amount of CMC is dissolved in the continuous phase, whereas lower concentrations would aggravate assessment of reliable relative viscosity data. The zero-shear viscosity of the CMC-solution as well as the graphite suspensions was obtained as the limiting constant viscosity value obtained at vanishing shear stresses. The relative viscosity $\eta_{r,0} = \eta_{0,suspension}/\eta_{0,solvent}$ of these graphite suspensions as a function of particle concentration is shown in Fig. 2d. This quantity exhibits a clear minimum around ϕ_p = 0.2 vol%, i.e. at a CMC to graphite volume ratio of 5 with a minimum value $\eta_{r,0} \approx 0.6$. In very dilute suspensions ($\phi_p \approx 10^{-2}$ vol%), however, $\eta_{r,0}$ approaches one, as expected. Interestingly, $\eta_{r,0}$ values are below 1 for $\phi_p < 5$ vol%. As confirmed by numerous theoretical and

experimental studies the relative viscosity η_r of suspensions increases with increasing particle loading and $\eta_r > 1$ always holds [57–60]. Therefore, another physical mechanism must control the low shear viscosity of the dilute graphite slurries investigated here. Li et al. showed a decrease of zeta potential for low concentrated graphite and CB suspensions upon addition of CMC, suggesting polymer adsorption on the particle surface [61]. Accordingly, the addition of graphite particles to the CMC solution decreases the polymer concentration in the fluid phase. The corresponding drop in $\eta_{0,suspension}$ is more pronounced than the weak increase in viscosity expected due to the added graphite, leading to relative viscosities below 1. At higher graphite concentration ($\phi_p > 5$ vol%), however, $\eta_{r,0}$ strongly increases because of the strong contribution of the particles to the suspensions viscosity. For $\phi_p = 20$ vol%, $\eta_{r,0}$ is even somewhat higher than 3, the value expected for non-Brownian hard sphere suspensions [55], and this is attributed to an increase in effective particle volume fraction due to the adsorbed CMC layer. In this concentration range the increase in $\eta_{0,suspension}$ with increasing particle concentration dominates over the drop in solvent viscosity due to the increasing fraction of CMC adsorbed to the particles when ϕ_p increases.

Electrical conductivity

Anode slurries were coated on glass plates and dried to investigate their electrical conductivity. Figure 3a shows corresponding data for layers including different CMC concentration and constant DS = 0.9 as a function of M_w. Note, the conductivity is due to the formation of a conducive CB particle network [27, 28]. Anode layers including only graphite exhibit overall lower values and an analog dependence on CMC concentration, M_w and DS as the electrical conductivity of anodes comprising graphite and CB. Irrespective of CMC molecular weight, conductivity of the dry anode layers clearly decreases with increasing polymer concentration as expected since the polymer can deteriorate and interrupt conductive pathways. However, the polymer molecular weight obviously has a significant impact on conductivity too. At given ϕ_{CMC}, the absolute values obtained for the layers including the CMC with M_w = 700 kDa are about 50% higher than that for the layers prepared using CMC with M_w = 250 kDa. It is well known from literature and it is also obvious from our rheological investigations discussed above that the mass of polymer adsorbed to the particle surface increases with increasing molecular weight [62–64]. Consequently, the fraction of CMC randomly distributed in the dried samples decreases with increasing M_w and it seems this fraction deteriorates the electrical conductivity of the anode layers investigated here. This new insight into the adsorption behavior of CMC with different polymer chain-length and its relationship to particle dispersion and electrical conductivity offers a path to increase conductivity through targeted choice of CMC molecular architecture at constant ϕ_{CMC}. Hence, power and energy density of corresponding cells might be improved. Finally, it should be noted that the degree of substitution has no significant effect on dry anode layer conductivity irrespective of CMC concentration (data not shown). This is in good agreement with rheological data indicating a weak effect of DS on low and high shear viscosity of the wet anode slurry.

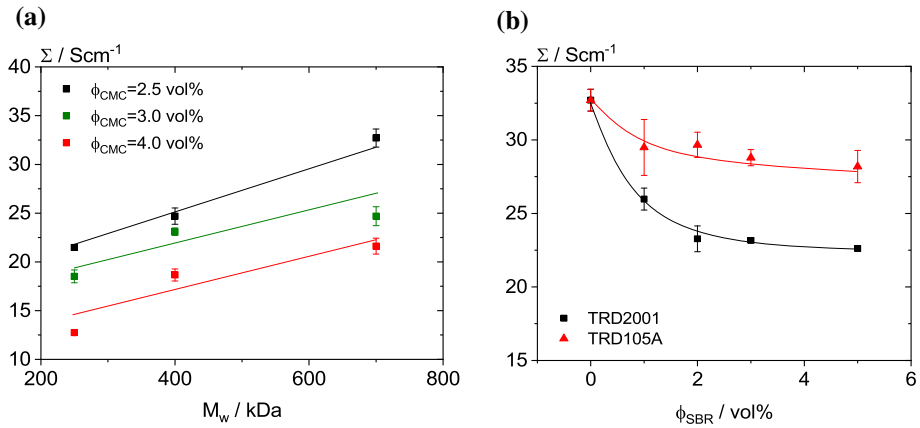

Figure 3 Electrical conductivity of dry electrode layers as a function of M_w including CMC at different concentrations and constant DS = 0.9 (**a**) as well as of ϕ_{SBR} including CMC with constant ϕ_{CMC} = 2.5 vol%, M_w = 700 kDa and DS = 0.9 but varying SBR-type.

Considering the high conductivity values of anodes including CMC at low concentration and high molecular weight, the influence of SBR type and concentration on the electrical conductivity of anode layers was investigated at constant ϕ_{CMC} = 2.5 vol%, M_w = 700 kDa and DS = 0.9 (Fig. 3b). Increasing ϕ_{SBR} leads to a monotonic decrease of electrical conductivity. Rheological data of corresponding wet slurries showed no significant effect of SBR on the flow behavior, i.e. variation of ϕ_{SBR} hardly affects particle dispersion and polymer adsorption. Hence, the decay in electrical conductivity is assumed to be a consequence of randomly distributed isolating polymer particles, blocking conductive pathways. Interestingly, anodes including TRD105A yield overall higher values than those of anodes based on TRD2001. This might be due to the smaller particle size or due to proprietary differences in polymer architecture or specific electrical properties. Elucidating this is, however, beyond the scope of this work focusing on the role of CMC as binder for LiB electrodes.

Mechanical properties and electrode microstructure

Adhesion

The influence of CMC on the adhesive strength between electrode layer and copper foil was investigated using the 90°-peel test. In all cases complete detachment of the anode layer from the current collector was observed (see supporting information). Figure 4a shows the line load of the measured samples over DS at constant M_w = 250 kDa, whereas Fig. 4b displays line load data as function of M_w at constant DS = 0.9, in both cases ϕ_{CMC} was varied between 2.5 and 4 vol%. Considering the experimental uncertainty of the measurements there is no significant dependence of adhesive strength on M_w or DS. In all investigated cases, the adhesive strength between electrode layer and current collector lies between 0.6 and 1.8 Nm^{-1}, and it must be noticed that the obtained values are more than one order of magnitude lower than that for water-based anodes containing an additional latex or rubber as binder system in combination with CMC [35, 43, 65]. This clearly shows that CMC hardly contributes to adhesion and that the addition of a second polymer is essential for the bond strength between electrode layer and current collector. Peel tests performed for SBR films on copper foils showed an average line load of 948 ± 47 Nm^{-1} and 832 ± 53 Nm^{-1} for TRD2001 and TRD105A, respectively, whereas CMC films, irrespective of M_w and DS, yielded only an average of 2.3 ± 0.7 Nm^{-1}. Accordingly, the intrinsic contribution of SBR to the adhesion of a LiB electrode is dramatically higher than that of CMC. The addition of SBR significantly enhances the adhesion between anode layer and current collector, increasing linearly with incrementing ϕ_{SBR} (see supporting information). SBR concentrations above 3.0 vol% yield adhesive strength values typical for aqueous anode layers reported in the literature [35, 65] (Fig. 4b).

Cohesion

In this section the cohesive strength of thick electrode layers is discussed focusing on the effect of added CMC. Different well-defined mechanical load types were employed to determine the critical stress at which the structure collapses. Results for layers including different concentrations of CMC with M_w = 250 kDa and DS = 0.9 are summarized in Fig. 5. Irrespective of load type the respective maximum stress increases almost linearly with increasing ϕ_{CMC}. The absolute value of σ_{max} depends on the nature of the load, i.e. it depends on whether the material is being pushed together, pulled apart, bent or twisted. The relative change in failure stress, however, is almost independent of load type. All test methods yield reliable and reproducible results and are therefore, suitable to characterize the cohesive strength of thick electrode layers. For the first time, cohesive and adhesive strength of electrode layers is determined independently. This should help to understand the delamination and cracking behavior due to cyclic lithium intercalation. For sake of convenience we will discuss the compressive strength in the subsequent part of this section. The other methods yielded similar trends upon variation of sample composition (see supporting information).

The porosity of thick electrode layers, used to investigate the cohesive strength, was measured and compared to that of thin layers used for electrical conductivity and adhesion measurements. The overall porosity of all samples was between 55 and 58%, showing no particular influence of CMC concentration, M_w, or DS. Similar results were reported in the literature for other water-borne LiB anodes. Thus, a

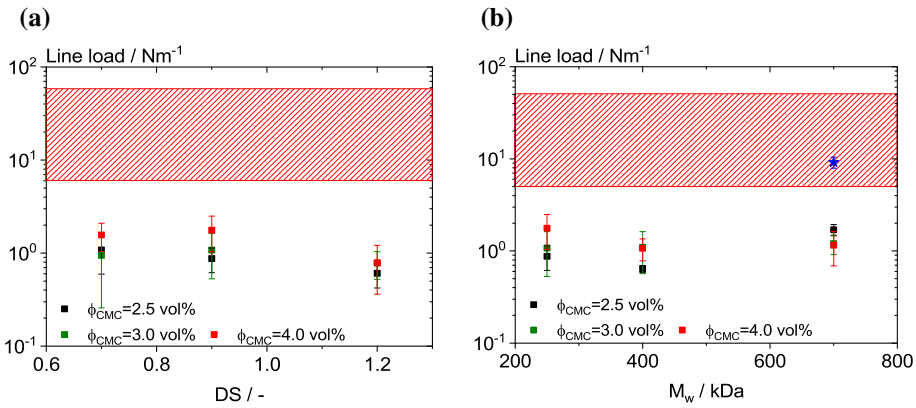

Figure 4 Adhesive strength of electrode layers including different CMC concentration as a function of **a** DS at constant M_w = 250 kDa and **b** M_w at constant DS = 0.9. Red hatched area denotes the line load of water-borne anode layers including graphite as active material and CMC as well as SBR as binder system [35, 65]. The blue star in the red hatched area indicates the adhesive strength of anode layers including CMC (ϕ_{CMC} = 2.5 vol%, M_w = 700 kDa, DS = 0.9) and the SBR binder TRD2001 at ϕ_{SBR} = 3.0 vol%.

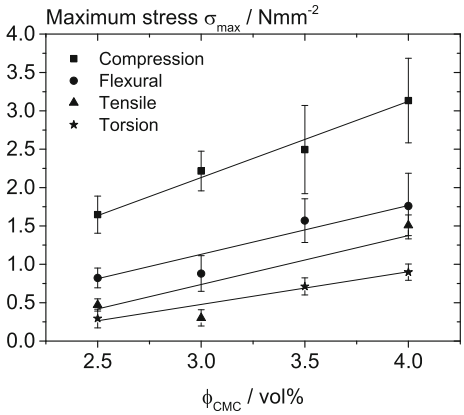

Figure 5 Maximum stress at break of thick electrode layers as a function of ϕ_{CMC} measured employing different load types. Samples including CMC with constant M_w = 250 kDa and DS = 0.9 were investigated.

significant influence of the sample porosity on the measured cohesive strength of thick electrode layers can be disregarded. Additionally, SEM images of thin and thick electrode layers exhibit no recognizable difference in their microstructure (see supporting information). Accordingly, the measured cohesive strength of thick electrode layers, investigated in this work, is assumed to be representative for conventional electrode layers.

Figure 6a displays the compressive strength of thick electrode layers including CMC with M_w = 250 kDa as a function of DS and Fig. 6b shows the compressive strength as a function of M_w at constant DS = 0.9. In both cases data were obtained at various ϕ_{CMC} between 2.5 and 4 vol%. First, it should be noted that the cohesive strength of pure CMC films neither depends on M_w nor on DS as directly confirmed by tensile test results obtained for the CMC grades investigated here (see supporting information).

The cohesive strength of electrode layers, however, strongly depends on these molecular parameters. On one hand, it significantly decreases with increasing DS. This decay is more pronounced at higher ϕ_{CMC}, and for DS = 1.2 the compressive strength hardly varies with ϕ_{CMC}. Adsorption isotherms for CMC on graphite particles show higher adsorption values for CMC with lower DS [16] corresponding to a lower solubility in water. Our results clearly show that this also has an effect on mechanical strength of the electrode layer and we assume that this is due to different particle dispersion and dry electrode layer microstructure depending on DS.

On the other hand, the cohesive strength of the thick dry layers increases with increasing M_w, particularly at high ϕ_{CMC}. The high cohesive strength obtained at high M_w again seems to be related to the higher fraction of CMC adsorbed on the surface of the graphite particles (s. Figure 2c). We hypothesize that the CMC molecular weight and the related variation in adsorption to the graphite and CB particles has a strong impact on particle dispersion as already indicated by its impact on slurry viscosity and in turn on microstructure and mechanical strength of the dry layer. This will be discussed in the next section. These findings indicate that electrode cohesion can be significantly increased without

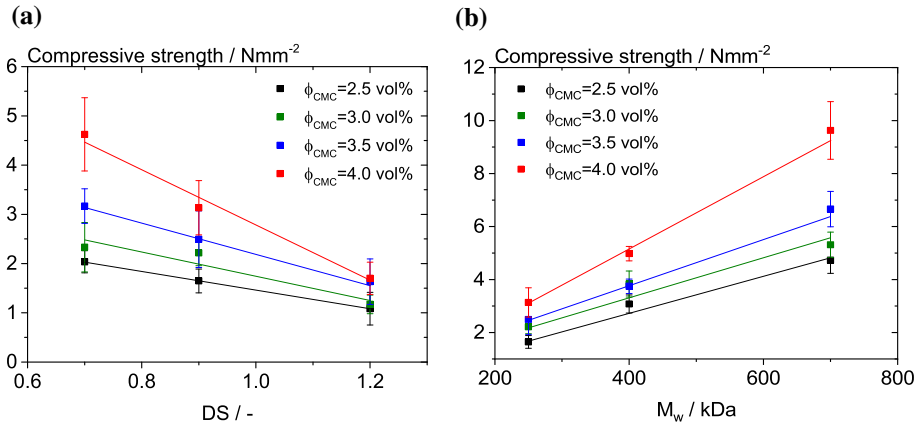

Figure 6 Maximum compressive strength of thick electrode layers including different CMC concentrations as a function of **a** DS at constant M_w = 250 kDa and **b** M_w at constant DS = 0.9.

increasing CMC concentration but through proper choice of molecular structure.

Finally, it should be noted that SBR does not contribute to the cohesive strength of thick anode layers irrespective of amount or type of added SBR (see supporting information). This is partly due to its lower intrinsic strength. Tensile tests performed on pure SBR films based on the standard DIN ISO EN 527-4 yielded intrinsic mechanical strength values of 4.3 ± 0.7 Nm m^{-2} and 9.2 ± 1.4 Nm m^{-2} for TRD2001 and TRD105A, respectively, whereas for CMC values > 15 N mm^{-2} were obtained, irrespective of M_w and DS. In addition, previous work [66] indicated that the addition of nanoparticulate secondary polymers hardly affects the electrode microstructure, which in turn controls the cohesive strength.

Microstructure

As already mentioned above, the porosity of all investigated samples was in the range between 55 and 58% irrespective of CMC concentration, M_w or DS. In more detail, SEM images of thick electrode layers were taken to investigate their microstructure. As shown by compression tests, a significant influence of M_w on the cohesive strength is obtained for ϕ_{CMC} = 4.0 vol% and DS = 0.9. Hence, SEM images of thick layers including 4 vol% CMC with M_w = 250 kDa and M_w = 700 kDa (DS = 0.9 in both cases) were compared (Fig. 7a, b). Electrodes including the low molecular-weight CMC show a random orientation of the flake-shaped graphite particles, whereas corresponding electrodes containing high molecular-weight CMC exhibit a clear particle alignment. Image processing was carried out for both images to quantify this observation. Individual particles and particle collectives were detected and their angle of orientation in relation to a centered coordinate system was noted, as marked in red (Fig. 7a, b). The particle frequency as a function of the orientation angle for samples including CMC with M_w = 250 kDa, M_w = 400 kDa and M_w = 700 kDa at constant DS = 0.9 is shown in Fig. 7c, d and e, respectively. For the M_w = 250 kDa sample, image analysis yields a broad distribution of particle orientation i.e. a random isotropic layer structure. In contrast, high molecular-weight CMC (M_w = 700 kDa) leads to particle alignment as confirmed by a narrow distribution of particle orientation angle. This kind of organized microstructure apparently correlates to the high cohesion values obtained for thick electrode layers based on M_w = 700 kDa CMC. Anodes including CMC with M_w = 400 kDa show an intermediate degree of particle orientation relative to those of anodes based on low and high M_w. This systematic change in particle alignment correlates to the linear increase of cohesive strength with increasing polymer chain-length, i.e. particle orientation.

Furthermore, SEM images of thick electrode layers including CMC at ϕ_{CMC} = 4 vol% and constant M_w = 250 kDa, but varying DS (DS = 0.7, DS = 0.9, and DS = 1.2) were compared to investigate the influence of DS on the microstructure of these layers. The corresponding histograms are shown in Fig. 7c, f and g. Electrode layers based on CMC with DS = 0.7 result in a narrow distribution of the particle orientation angles, indicating clear particle alignment. Intermediate DS leads to a weak particle alignment towards 100°, whereas the highest DS results in randomly oriented particles, i.e. a broad uniform distribution of orientation angles. Analog with the results

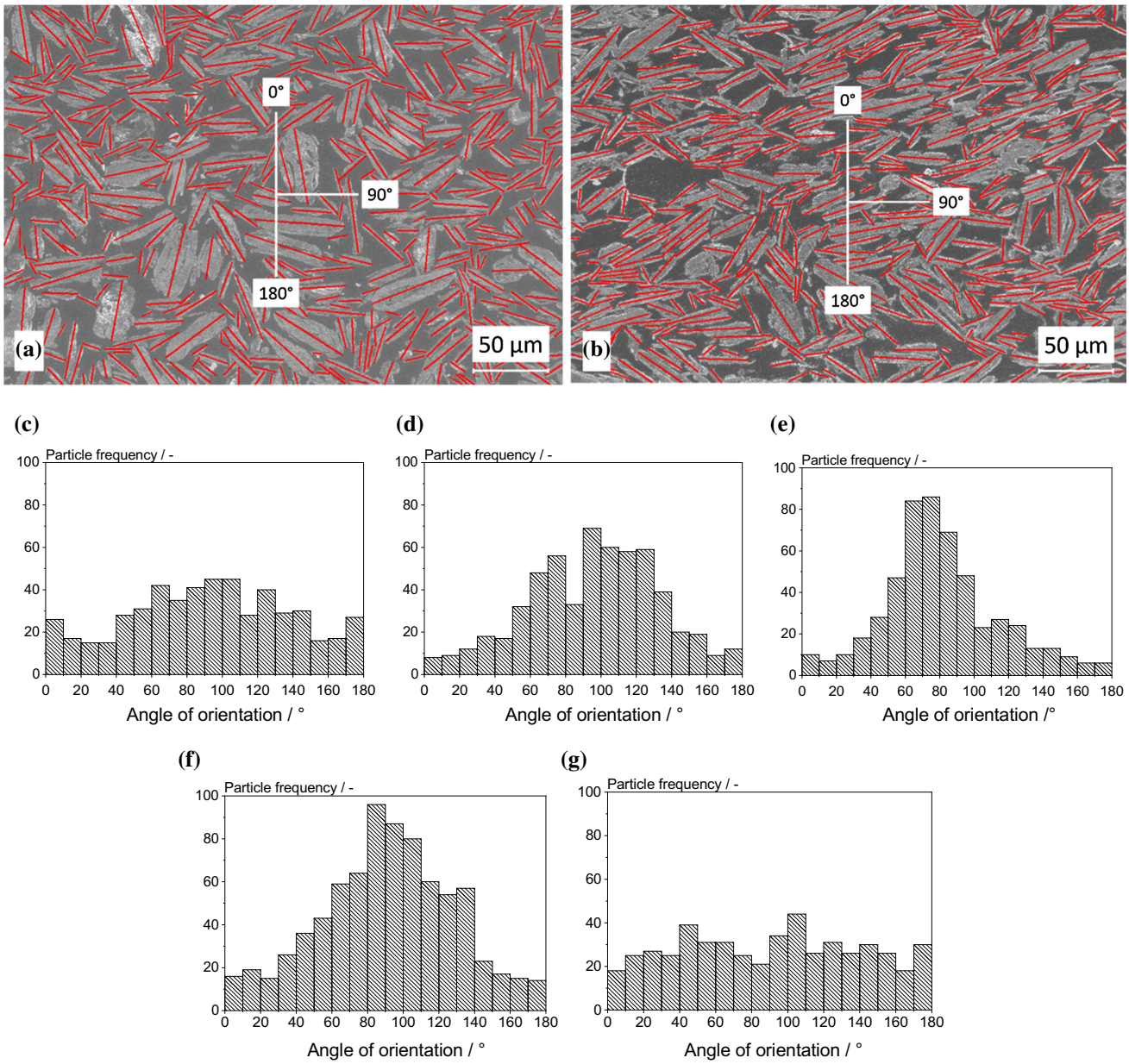

Figure 7 Microstructure of thick electrode layers. **a** SEM image of layer including ϕ_{CMC} = 4 vol% CMC with DS = 0.9 and M_w = 250 kDa and **b** M_w = 700 kDa. Histograms of particle frequency as a function of angle of orientation relative to the coordinate system indicated by the white line in A and B in thick electrode layers including CMC with **c** M_w = 250 kDa, **d** M_w = 400 kDa and **e** M_w = 700 kDa at constant DS = 0.9 as well as CMC with **f** DS = 0.7 and **g** DS = 1.2 at constant M_w = 250 kDa.

obtained for electrode layers comprising CMC with different M_w, the particle orientation in the electrode layer correlates to the cohesive strength when using different DS. These results demonstrate that the cohesive strength of electrode layers is determined by the microstructure formed due to the added CMC. This structure and hence the mechanical strength of the layers strongly depends on M_w and DS of the added CMC, although the intrinsic mechanical strength of CMC itself does not depend on these parameters. The high degree of particle alignment at high M_w and low DS is presumably promoted by the lower viscosity of the continuous phase of the corresponding slurry as a result of the higher fraction of CMC adsorbed on the particles.

Conclusions

Here we investigated the effect of CMC, which is widely used as a binder and rheology control agent in waterborne LiB electrode slurries, on the flow behavior of anode slurries as well as on the electrical and mechanical properties and finally also the microstructure of the corresponding dry layers. CMC concentration, M_w and DS were systematically varied in a wide technically relevant range. In addition, the influence of SBR type and concentration on the features mentioned above was discussed. This holistic approach establishes new insights into the polymer adsorption behavior on active particles at industrially relevant slurry concentrations as well as clear correlations between particle dispersion, layer microstructure as well as electrical conductivity and mechanical integrity of the electrode.

Shear rheometry revealed that both, low and high shear viscosity strongly increase with M_w up to 400 kDa and then level off irrespective of the amount of added CMC but, as expected, the absolute viscosity values monotonically increase with ϕ_{CMC}. Moreover, the relative high shear viscosity $\eta_{r,\infty}$ is essentially independent of ϕ_{CMC} but monotonically decreases with increasing M_w. We attribute this effect to the partial adsorption of CMC on the solid particles and the corresponding loss of polymer in the solvent. Obviously, the loss of dissolved polymer is more pronounced for higher M_w, as expected [62–64]. This phenomenon was further supported considering the relative viscosity of graphite suspension in a CMC solution covering a broad range of particle loading. The higher affinity of CMC to the graphite surface at lower DS also shows up in the rheological data. Finally, the addition of SBR does not affect the flow behavior of anode slurries.

The electrical conductivity decreased with increasing ϕ_{CMC} as expected, but strikingly conductivity substantially increased with increasing M_w at fixed ϕ_{CMC}. Since the fraction of adsorbed CMC increases with increasing M_w we hypothesize that the remaining free polymer deteriorates the formation of a percolating CB network and hence the conductivity of the dry anode layers. Accordingly, adding CMC with high M_w at constant ϕ_{CMC} results in an increase of electrical conductivity, which is associated to cell power and energy density. The weak changes of CMC adsorption with varying DS did not show up in dry layer conductivity. As expected, increasing SBR concentration also resulted in a monotonic decay of electrical conductivity.

The adhesive strength of dry layers including CMC as only binder component to copper foils is about two orders of magnitude lower than that of conventional, water-based anode layers including a secondary binder and hardly varies with ϕ_{CMC}, M_w or DS. Obviously, CMC does not contribute to the adhesive strength of LiB anode layers. Addition of SBR leads to a linear increase of adhesion at the interface, highlighting the role of rubber-like polymer binders.

The cohesive strength of dry electrode layers has to balance the mechanical stress during cyclic intercalation of Li-ions in the layers, and is supposed to be related to cracking and mechanical failure of battery electrodes. We investigated this phenomenon employing different load types to characterize the critical stress σ_{max} at which thick electrode layers break. As expected, σ_{max} significantly increases with ϕ_{CMC} and all employed test methods yielded reliable results. Preliminary porosity measurements and SEM-images confirmed, that the microstructure of the thick layers was similar to that of the thin layers investigated regarding electrical conductivity and adhesive strength. Therefore, we consider the results of these cohesion tests relevant also for thin LiB electrode layers, rendering first cohesion values for water-based anodes determined under well-defined mechanical load conditions independent of electrode adhesive strength.

Although the mechanical strength of pure CMC films neither depends on M_w nor on DS, we found a strong dependence of compressive strength of electrode layers on both parameters: σ_{max} decreases with increasing DS but strongly increases with increasing M_w, i.e. with increasing fraction of adsorbed CMC. Apparently, the degree of CMC adsorption on graphite particles also must have a strong impact on the microstructure determining the mechanical strength of the dry layers. This change in microstructure was directly visualized using scanning electron microscopy. Image analysis of these micrographs revealed a strong orientation of graphite particles for layers including CMC with high M_w or low DS, i.e. when a larger fraction of CMC is adsorbed on the particle surface. This effect of CMC adsorption also seems to be decisive for the electrical conductivity of these layers. Contrary to its effect on adhesive strength, the addition of SBR has no influence on the cohesive strength.

In summary, the variation of CMC architecture (M_w, DS) and the corresponding change in adsorption on graphite particles not only affects the flow behavior and hence processing properties of the anode slurries but also the microstructure of the dry layers and hence their electrical conductivity as well as cohesive strength. The holistic study presented in this work renders a comprehensive and systematic understanding of the role of CMC in water-based anodes for LiB, unveiling clear correlations between polymer/particle interactions and resulting electrode properties. Accordingly, the targeted choice of CMC is supposed to be decisive not only for fabrication but also for electrical performance and long-term mechanical stability of LiB electrodes.

Acknowledgements

Open Access funding provided by Projekt DEAL. R. Gordon gratefully acknowledges financial support by the *100 prozent erneuerbar Stiftung*. Special thanks go to H. Balmer, H. Mild, A. Laghmani and A. García for their experimental assistance and data analysis.

Electronic supplementary material: The online version of this article (https://doi.org/10.1007/s10853-020-05122-3) contains supplementary material, which is available to authorized users.

References

[1] Goriparti S, Miele E, De Angelis F, Di Fabrizio E, Proietti Zaccaria R, Capiglia C (2014) Review on recent progress of nanostructured anode materials for Li-ion batteries. J Power Sources 257:421–443

[2] Luo X, Wang J, Dooner M, Clarke J (2015) Overview of current development in electrical energy storage technologies and the application potential in power system operation. Appl Energy 137:511–536

[3] Nitta N, Wu F, Lee JT, Yushin G (2015) Li-ion battery materials: present and future. Mater Today 18(5):252–264

[4] Deng D (2015) Li-ion batteries: basics, progress, and challenges. Energy Sci Eng 3(5):385–418

[5] Blomgren GE (2017) The development and future of lithium ion batteries. J Electrochem Soc 164(1):A5019–A5025

[6] Liu C, Li F, Lai-Peng M, Cheng HM (2010) Advanced materials for energy storage. Adv Mater 22(8):28–62

[7] Cheng F, Liang J, Tao Z, Chen J (2011) Functional materials for rechargeable batteries. Adv Mater 23(15):1695–1715

[8] Croguennec L, Palacin MR (2015) Recent achievements on inorganic electrode materials for lithium-ion batteries. J Am Chem Soc 137(9):3140–3156

[9] Roy P, Srivastava SK (2015) Nanostructured anode materials for lithium ion batteries. J Mater Chem A 3(6):2454–2484

[10] Schon TB, McAllister BT, Li PF, Seferos DS (2016) The rise of organic electrode materials for energy storage. Chem Soc Rev 45(22):6345–6404

[11] Maleki H, Deng G, Kerzhner-Haller I, Anani A, Howard JN (2000) Thermal stability studies of binder materials in anodes for lithium-ion batteries. J Electrochem Soc 147(12):4470–4475

[12] Zhang X et al (2001) Diagnostic characterization of high power lithium-ion batteries for use in hybrid electric vehicles. J Electrochem Soc 148(5):A463–A470

[13] Wood DL, Li J, Daniel C (2015) Prospects for reducing the processing cost of lithium ion batteries. J Power Sources 275:234–242

[14] Wood DL, Quass JD, Li J, Ahmed S, Ventola D, Daniel C (2018) Technical and economic analysis of solvent-based lithium-ion electrode drying with water and NMP. Dry Technol 36(2):234–244

[15] Lee JH, Lee S, Paik U, Choi YM (2005) Aqueous processing of natural graphite particulates for lithium-ion battery anodes and their electrochemical performance. J Power Sources 147(1–2):249–255

[16] Lee J-H, Paik U, Hackley VA, Choi Y-M (2005) Effect of carboxymethyl cellulose on aqueous processing of natural graphite negative electrodes and their electrochemical

performance for lithium batteries. J Electrochem Soc 152(9):A1763–A1769

[17] Liu W-R, Yang M-H, Wu H-C, Chiao SM, Wu N-L (2005) Enhanced cycle life of si anode for Li-ion batteries by using modified elastomeric binder. Electrochem Solid State Lett 8(2):A100

[18] Buqa H, Holzapfel M, Krumeich F, Veit C, Novák P (2006) Study of styrene butadiene rubber and sodium methyl cellulose as binder for negative electrodes in lithium-ion batteries. J Power Sources 161(1):617–622

[19] Lee JH, Choi YM, Paik U, Park JG (2006) The effect of carboxymethyl cellulose swelling on the stability of natural graphite particulates in an aqueous medium for lithium ion battery anodes. J Electroceram 17(2–4):657–660

[20] Li J, Lewis RB, Dahn JR (2007) Sodium carboxymethyl cellulose. Electrochem Solid State Lett 10(2):A17–A20

[21] Kulicke WM, Kull AH, Kull W, Thielking H, Engelhardt J, Pannek JB (1996) Characterization of aqueous carboxymethylcellulose solutions in terms of their molecular structure and its influence on rheological behaviour. Polymer (Guildf) 37(13):2723–2731

[22] Kästner U, Hoffmann H, Dönges R, Hilbig J (1997) Structure and solution properties of sodium carboxymethyl cellulose. Colloids Surf A Physicochem Eng Asp 123–124(1993):307–328

[23] Hoogendam CW, de Keizer A, Cohen Stuart MA, Bijsterbosch BH, Batelaan JG, van der Horst PM (1998) Adsorption mechanisms of carboxymethyl cellulose on mineral surfaces. Langmuir 14(14):3825–3839

[24] Barbucci R, Magnani A, Consumi M (2000) Swelling behavior of carboxymethylcellulose hydrogels in relation to cross-linking, pH, and charge density. Macromolecules 33(20):7475–7480

[25] Truzzolillo D, Bordi F, Cametti C, Sennato S (2009) Counterion condensation of differently flexible polyelectrolytes in aqueous solutions in the dilute and semidilute regime. Phys Rev E Stat Nonlinear Soft Matter Phys 79(1):1–9

[26] Lopez CG, Rogers SE, Colby RH, Graham P, Cabral JT (2015) Structure of sodium carboxymethyl cellulose aqueous solutions: a SANS and rheology study. J Polym Sci Part B Polym Phys 53(7):492–501

[27] Guy D, Lestriez B, Bouchet R, Guyomard D (2006) Critical role of polymeric binders on the electronic transport properties of composites electrode. J Electrochem Soc 153(4):A679–A688

[28] Lestriez B (2010) Functions of polymers in composite electrodes of lithium ion batteries. C R Chim 13(11):1341–1350

[29] Liu G, Zheng H, Song X, Battaglia VS (2012) Particles and polymer binder interaction: a controlling factor in lithium-ion electrode performance. J Electrochem Soc 159(3):A214–A221

[30] Arora P (1998) Capacity fade mechanisms and side reactions in lithium-ion batteries. J Electrochem Soc 145(10):3647–3667

[31] Hao F, Fang D (2013) Reducing diffusion-induced stresses of electrode-collector bilayer in lithium-ion battery by prestrain. J Power Sources 242:415–420

[32] Rahani EK, Shenoy VB (2013) Role of plastic deformation of binder on stress evolution during charging and discharging in lithium-ion battery negative electrodes. J Electrochem Soc 160(8):A1153–A1162

[33] Yoo M, Frank CW, Mori S, Yamaguchi S (2003) Effect of poly(vinylidene fluoride) binder crystallinity and graphite structure on the mechanical strength of the composite anode in a lithium ion battery. Polymer (Guildf) 44(15):4197–4204

[34] Kim K, Byun S, Cho I, Ryou MH, Lee YM (2016) Three-dimensional adhesion map based on surface and interfacial cutting analysis system for predicting adhesion properties of composite electrodes. ACS Appl Mater Interfaces 8(36):23688–23695

[35] Baunach M, Jaiser S, Schmelzle S, Nirschl H, Scharfer P, Schabel W (2016) Delamination behavior of lithium-ion battery anodes: influence of drying temperature during electrode processing. Dry Technol 34(4):462–473

[36] Shin D, Park H, Paik U (2017) Cross-linked poly(acrylic acid)-carboxymethyl cellulose and styrene–butadiene rubber as an efficient binder system and its physicochemical effects on a high energy density graphite anode for Li-ion batteries. Electrochem Commun 77:103–106

[37] Hernandez CR et al (2018) A facile and very effective method to enhance the mechanical strength and the cyclability of si-based electrodes for Li-ion batteries. Adv Energy Mater 8(6):1–13

[38] Jeschull F, Brandell D, Wohlfahrt-Mehrens M, Memm M (2017) Water-soluble binders for lithium-ion battery graphite electrodes: slurry rheology, coating adhesion, and electrochemical performance. Energy Technol 5(11):2108–2118

[39] Chen Z, Christensen L, Dahn JR (2003) Large-volume-change electrodes for Li-ion batteries of amorphous alloy particles held by elastomeric tethers. Electrochem Commun 5(11):919–923

[40] Chen L, Xie X, Xie J, Wang K, Yang J (2006) Binder effect on cycling performance of silicon/carbon composite anodes for lithium ion batteries. J Appl Electrochem 36(10):1099–1104

[41] Lee JT, Chu YJ, Peng XW, Wang FM, Yang CR, Li CC (2007) A novel and efficient water-based composite binder

for $LiCoO_2$ cathodes in lithium-ion batteries. J Power Sources 173(2):985–989
[42] Park HK, Kong BS, Oh ES (2011) Effect of high adhesive polyvinyl alcohol binder on the anodes of lithium ion batteries. Electrochem Commun 13(10):1051–1053
[43] Son B et al (2014) Measurement and analysis of adhesion property of lithium-ion battery electrodes with SAICAS. ACS Appl Mater Interfaces 6(1):526–531
[44] Zhang Z, Zeng T, Lai Y, Jia M, Li J (2014) A comparative study of different binders and their effects on electrochemical properties of $LiMn_2O_4$ cathode in lithium ion batteries. J Power Sources 247:1–8
[45] Haselrieder W, Westphal B, Bockholt H, Diener A, Höft S, Kwade A (2015) Measuring the coating adhesion strength of electrodes for lithium-ion batteries. Int J Adhes Adhes 60:1–8
[46] Zhong H, He A, Lu J, Sun M, He J, Zhang L (2016) Carboxymethyl chitosan/conducting polymer as water-soluble composite binder for $LiFePO_4$ cathode in lithium ion batteries. J Power Sources 336:107–114
[47] Lee BR, Oh ES (2013) Effect of molecular weight and degree of substitution of a sodium-carboxymethyl cellulose binder on $Li_4Ti_5O_{12}$ anodic performance. J Phys Chem C 117(9):4404–4409
[48] Wu M et al (2013) Toward an ideal polymer binder design for high-capacity battery anodes. J Am Chem Soc 135(32):12048–12056
[49] Chen J, Liu J, Qi Y, Sun T, Li X (2013) Unveiling the roles of binder in the mechanical integrity of electrodes for lithium-ion batteries. J Electrochem Soc 160(9):A1502–A1509
[50] Babinec S, Tang H, Talik A, Hughes S, Meyers G (2007) Composite cathode structure/property relationships. J Power Sources 174(2):508–514
[51] Zheng H, Zhang L, Liu G, Song X, Battaglia VS (2012) Correlationship between electrode mechanics and long-term cycling performance for graphite anode in lithium ion cells. J Power Sources 217:530–537
[52] Antartis D, Dillon S, Chasiotis I (2015) Effect of porosity on electrochemical and mechanical properties of composite Li-ion anodes. J Compos Mater 49(15):1849–1862
[53] Bitsch B, Willenbacher N, Wenzel V, Schmelzle S, Nirschl H (2015) Einflüsse der mechanischen verfahrenstechnik auf die herstellung von elektroden für lithium-ionen-batterien. Chem Ing Tech 87(4):466–474
[54] Smits FM (1958) Measurement of sheet resistivities with the four-point probe. Bell Syst Tech J 37(3):711–718
[55] Mewis J, Wagner NJ (2011) Colloidal suspension rheology. Cambridge University Press, Cambridge
[56] Rubinstein M, Colby RH (2003) Polymer physics. Polymer International, London
[57] Krieger IM, Dougherty TJ (1959) A mechanism for non-Newtonian flow in suspensions of rigid spheres. Trans Soc Rheol 3(1):137–152
[58] Batchelor GK, Green JT (1972) The effect of Brownian motion on the bulk stress in a suspension of spherical particles. J Fluid Mech 56(3):401–427
[59] Quemada D (1977) Rheology of concentrated disperse systems and minimum energy dissipation. Rheol Acta 16:82–94
[60] Meeker SP, Poon WCK, Pusey PN (1997) Concentration dependence of the low-shear viscosity of suspensions of hard-sphere colloids. Phys Rev E Stat Phys Plasmas Fluids Relat Interdiscip Top 55(5):5718–5722
[61] Li C-C, Lin Y-S (2012) Interactions between organic additives and active powders in water-based lithium iron phosphate electrode slurries. J Power Sources 220:413–421
[62] Roe RJ (1974) Multilayer theory of adsorption from a polymer solution. J Chem Phys 4192(8):4192–4207
[63] Scheutjens JMHM, Fleer GJ (1979) Statistical theory of the adsorption of interacting chain molecules. 1. Partition function, segment density distribution, and adsorption isotherms. J Phys Chem 83(12):1619–1635
[64] Scheutjens JMHM, Fleer GJ (1980) Statistical theory of the adsorption of interacting chain molecules. 2. Train, loop, and tail size distribution. J Phys Chem 84(2):178–190
[65] Park J, Willenbacher N, Ahn KH (2019) How the interaction between styrene–butadiene-rubber (SBR) binder and a secondary fluid affects the rheology, microstructure and adhesive properties of capillary-suspension-type graphite slurries used for Li-ion battery anodes. Colloids Surf A Physicochem Eng Asp 579:123692
[66] Gordon R, Kassar M, Willenbacher N (2020) Effect of polymeric binders on dispersion of active particles in aqueous $LiFePO_4$-based cathode slurries as well as on mechanical and electrical properties of corresponding dry layers. ACS Omega. https://doi.org/10.1021/acsomega.0c00477